Appl. Numer. Math. 205 (2024) 87–100

Contents lists available at ScienceDirect

Applied Numerical Mathematics

journal homepage: www.elsevier.com/locate/apnum

Research Paper

The enriched multinode Shepard collocation method for solving elliptic problems with singularities

Francesco Dell'Accio [a], Filomena Di Tommaso [a], Elisa Francomano [b,*]

[a] Department of Mathematics and Computer Science, University of Calabria, Rende (CS), Italy
[b] Department of Engineering, University of Palermo, Palermo, Italy

ARTICLE INFO

Keywords:
Approximation by rational functions
Multinode Shepard method
Collocation method
Elliptic PDEs
Motz problem

ABSTRACT

In this paper, the multinode Shepard method is adopted for the first time to numerically solve a differential problem with a discontinuity in the boundary. Starting from previous studies on elliptic boundary value problems, here the Shepard method is employed to catch the singularity on the boundary. Enrichments of the functional space spanned by the multinode cardinal Shepard basis functions are proposed to overcome the difficulties encountered. The Motz's problem is considered as numerical benchmark to assess the method. Numerical results are presented to show the effectiveness of the proposed approach.

1. Introduction

The Motz's problem was introduced in 1947 [1] to analyze the performance of the relaxation method and it is considered a benchmark to verify the efficiency of numerical schemes in solving elliptic problems with singular boundary conditions [2]. The problem, whose formulation has been modified by Wait and Mitchell [3] in 1971, consists in finding the solution of the Laplace equation

$$\Delta u = 0 \tag{1}$$

in the rectangular domain

$$\Omega = \{(x, y) : -1 < x < 1, 0 < y < 1\}$$

subject to the following mixed Neumann–Dirichlet boundary conditions (see Fig. 1 for a graphical representation)

$$\begin{cases} u = 0, & \text{if } y = 0 \quad \text{and} \quad -1 \le x < 0 \quad (\Gamma_1) \\ \frac{\partial u}{\partial y} = 0, & \text{if } y = 0 \quad \text{and} \quad 0 < x \le 1 \quad (\Gamma_2) \\ u = 500, & \text{if } x = 1 \quad \text{and} \quad 0 \le y \le 1 \quad (\Gamma_3) \\ \frac{\partial u}{\partial y} = 0, & \text{if } y = 1 \quad \text{and} \quad -1 < x < 1 \quad (\Gamma_4) \\ \frac{\partial u}{\partial x} = 0, & \text{if } x = -1 \quad \text{and} \quad 0 \le y \le 1 \quad (\Gamma_5). \end{cases} \tag{2}$$

* Corresponding author.
E-mail addresses: francesco.dellaccio@unical.it (F. Dell'Accio), filomena.ditommaso@unical.it (F. Di Tommaso), elisa.francomano@unipa.it (E. Francomano).

https://doi.org/10.1016/j.apnum.2024.07.005
Received 31 May 2024; Received in revised form 16 July 2024; Accepted 16 July 2024

Available online 20 July 2024

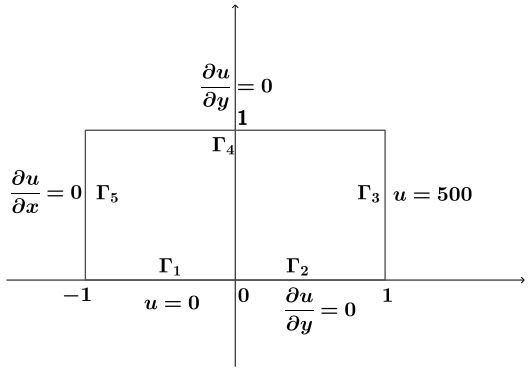

Fig. 1. Graphical representation of the boundary conditions in (2).

Table 1
First 20 coefficients of the series (3) provided by [8].

Coefficient	Value	Coefficient	Value
A_1	401.1624537452	A_{11}	0.0073023017
A_2	87.6559201951	A_{12}	−0.0031841139
A_3	17.2379150794	A_{13}	0.0012206461
A_4	−8.0712152597	A_{14}	0.0005309655
A_5	1.4402727170	A_{15}	0.0002715122
A_6	0.3310548859	A_{16}	−0.0001200463
A_7	0.2754373445	A_{17}	0.0000505400
A_8	−0.0869329945	A_{18}	0.000023167
A_9	0.0336048784	A_{19}	0.000011535
A_{10}	0.0153843745	A_{20}	−0.000005295

The solution $u(x, y)$ of the Motz's problem has a singularity at the point $(0, 0)$ [2] and it can be expressed as the sum of the series

$$u(r,\theta) = \sum_{i=1}^{\infty} A_i r^{i-\frac{1}{2}} \cos\left[\left(i - \frac{1}{2}\right)\theta\right], \tag{3}$$

where r and θ are the polar coordinates centered at the singular point [4]. In 1975 Rosser and Papamichael [5] show that the convergence radius of the series (3) is at least 2 and therefore the above expansion is valid in the whole solution domain $\Omega \cup \partial\Omega$. Moreover, they compute the first 20 coefficients A_i of the series (3) by using a conformal mapping technique. In 1996 Georgiou, Olson and Smyrlis [6] compute the first 25 coefficients by using a Singular Function Boundary Integral Method (SFBIM). The convergence of this method, which allows to get the coefficients of the asymptotic expansion at a exponential rate, has been studied in [7]. In 2004 Lu, Hu and Li [8] provide the first 34 coefficients A_i with great accuracy (17 significant digits for A_1) by using a collocation Trefftz method. Moreover, in 2006 Li, Chan, Georgiou and Xenophontos [9] solved the Motz problem using different boundary approximation methods and presented converged results for the leading 35 singular coefficients. The first 20 values of these coefficients are reported in Table 1.

Efficient standard numerical methods like finite element, boundary element, finite difference and spectral methods are typically employed in solving elliptic partial differential equations [10–13,3,14]. These methods, however, face challenges in handling problems with singularities, leading to a decline in their high-order convergence rates. Such singularities are commonly encountered in engineering problems, either due to sudden changes in boundary conditions on smooth boundaries or to the presence of re-entrant corners. To address the numerical solution challenges of elliptic problems with boundary singularities, the common strategy is a grid refinement near the singularity. While this approach can be effective, it significantly raises computational costs and does not always yield satisfactory efficiency.

An improved solution is to integrate analytical insights about the singularities directly into the numerical model. Following Motz's pioneering work, these specialized methods have been frequently employed to enhance the precision of traditional numerical approaches. The core concept involves employing the asymptotic solution form (3) close to the singularity and a standard numerical method for the remaining domain. The unknown coefficients of the asymptotic solution are determined by matching them with the numerical solution at specific boundary nodes. For two-dimensional Laplace and Poisson equations, such methods have been successfully applied in conjunction with finite difference and finite element techniques. In boundary element methods, the domain's entire solution is approximated using the leading terms of the local asymptotic expansion, with the expansion coefficients computed by minimizing the boundary condition residuals at selected boundary nodes [4,15–17].

Recently, methods capable to work with data irregularly distributed across the problem domain have been incrementally adopted to solve differential problems [18–21]. The multinode Shepard method [22] has been used to solve BVPs too [23,24] and it has proven to be an interesting computational alternative to the most commonly adopted methods [25–27]. In this paper, we extend the

multinode Shepard method by including additional enrichment functions to capture the singularity in solving the Motz's problem. The multinode cardinal Shepard basis is enriched with special functions allowing to catch the singularity at the origin giving the method more flexibility.

In order to keep the paper self-contained, in Section 2 the method is briefly explained and in Section 3 some numerical experiments are presented. In Section 4 the enriched multinode Shepard method is introduced and simulations are performed on different data sets to investigate the impact on the accuracy, by varying the number of enrichment functions.

2. Fundamentals on the multinode Shepard method

The multinode Shepard method allows the reconstruction of a function from scattered data in the multidimensional euclidean space by combining local interpolation polynomials of total degree with inverse distance weighted basis functions [28]. Since the specificity of Motz's problem, here we set $\Omega = (-1,1)\times(0,1)$. Let $\mathcal{S} = \{\boldsymbol{\eta}_1,\dots,\boldsymbol{\eta}_n\} \subset \bar{\Omega}$ with $\boldsymbol{\eta}_i \neq \boldsymbol{\eta}_j$, for $i \neq j$, $\mathcal{F} = \{f_1,\dots,f_n\}$ the known function values at the nodes $\boldsymbol{\eta}_i$ and $\Pi_r(\mathbb{R}^2)$ the space of bivariate polynomials of total degree r.

To construct the multinode Shepard operator we set

$$m = \frac{(r+1)(r+2)}{2} = \dim\left(\Pi_r(\mathbb{R}^2)\right)$$

and define injective maps

$$\phi_\tau : \{1,\dots,m\} \longrightarrow \{1,\dots,n\}, \quad \tau = 1,\dots,s,$$

with $\tau_\kappa := \phi_\tau(\kappa)$, and we consider a cover of $\mathcal{S}$ by means of subsets $\gamma_\tau = \{\boldsymbol{\eta}_{\tau_1},\dots,\boldsymbol{\eta}_{\tau_m}\}$, $\tau = 1,\dots,s$, for which it exists a unique polynomial $p_\tau(\boldsymbol{x}) \in \Pi_r(\mathbb{R}^2)$ such that

$$p_\tau(\boldsymbol{\eta}_{\tau_\kappa}) = f_{\tau_\kappa} \qquad \tau = 1,\dots,s, \quad \kappa = 1,\dots,m. \tag{4}$$

In practice, each set γ_τ is realized by selecting a subset of m discrete Leja points from a set of $m+q$, $q>0$ nearby nodes (for more details see [23,29,30]). The interpolant (4) is represented as

$$p_\tau(\boldsymbol{x}) = \sum_{\iota=1}^{m} \ell_{\tau,\iota}(\boldsymbol{x}) f_{\tau_\iota}, \qquad \boldsymbol{x} \in \mathbb{R}^2,$$

where $\ell_{\tau,\iota}(\boldsymbol{x})$ are the Lagrange fundamental polynomials expressed in the *Taylor basis* centered at the barycenter $\boldsymbol{\eta}_\tau^{(b)}$ of γ_τ, that is,

$$\ell_{\tau,\iota}(\boldsymbol{x}) = \sum_{|\alpha|\le r} a_\alpha^{(\tau,\iota)} \left(\boldsymbol{x} - \boldsymbol{\eta}_\tau^{(b)}\right)^\alpha, \tag{5}$$

with $\alpha \in \mathbb{Z}_+^2$ being a multi-index [31]. By considering the multinode basis functions related to the cover $\{\gamma_\tau\}_{\tau=1}^s$

$$K_{\nu,\tau}(\boldsymbol{x}) = \frac{\prod_{\iota=1}^{m} \left\|\boldsymbol{x} - \boldsymbol{\eta}_{\tau_\iota}\right\|^{-\nu}}{\sum_{l=1}^{s}\prod_{\beta=1}^{m} \left\|\boldsymbol{x} - \boldsymbol{\eta}_{l_\beta}\right\|^{-\nu}}, \qquad \tau = 1,\dots,s; \quad \nu > 0, \tag{6}$$

the multinode Shepard approximant is defined as follows

$$\mathcal{M}_\nu[f](\boldsymbol{x}) = \sum_{\tau=1}^{s} K_{\nu,\tau}(\boldsymbol{x})\, p_\tau(\boldsymbol{x}). \tag{7}$$

The functions $K_{\nu,\tau}(\boldsymbol{x})$ satisfy the following properties

1. $\sum_{\tau=1}^{s} K_{\nu,\tau}(\boldsymbol{x}) = 1, \quad \boldsymbol{x} \in \mathbb{R}^2$
2. $K_{\nu,\tau}(\boldsymbol{\eta}_\iota) = 0$ for all $\boldsymbol{\eta}_\iota \notin \gamma_\tau$
3. $\sum_{\tau\in\mathcal{T}_\iota} K_{\nu,\tau}(\boldsymbol{\eta}_\iota) = 1,$
4. $\nabla K_{\nu,\tau}(\boldsymbol{\eta}_\iota) = \boldsymbol{0}$ for all $\boldsymbol{\eta}_\iota \notin \gamma_\tau$, $\nu \in 2\mathbb{Z}_+$, $\nu > 1$
5. $\sum_{\tau\in\mathcal{T}_\iota} \nabla K_{\nu,\tau}(\boldsymbol{\eta}_\iota) = \boldsymbol{0}$, $\nu \in 2\mathbb{Z}_+$, $\nu > 1$
6. $\mathrm{H}\, K_{\nu,\tau}(\boldsymbol{\eta}_\iota) = \boldsymbol{0}$ for all $\boldsymbol{\eta}_\iota \notin \gamma_\tau$, $\nu \in 2\mathbb{Z}_+$, $\nu > 2$,
7. $\sum_{\tau\in\mathcal{T}_\iota} \mathrm{H}\, K_{\nu,\tau}(\boldsymbol{\eta}_\iota) = \boldsymbol{0}$, $\nu \in 2\mathbb{Z}_+$, $\nu > 2$

where $\nabla K_{\nu,\tau}(\boldsymbol{x})$ and $\mathrm{H}\,K_{\nu,\tau}(\boldsymbol{x})$ are the gradient and the Hessian matrix of $K_{\nu,\tau}$ and $\mathcal{T}_\imath$, $\imath = 1,\dots,n$, is the set of indices $\tau \in \{1,\dots,s\}$ such that $\boldsymbol{\eta}_\imath \in \gamma_\tau$.

The properties 1-3 imply that $\mathcal{M}_\nu[f]$ interpolates $f_\imath$, $\imath = 1,\dots,n$, and $\mathcal{M}_\nu[p] = p$ for all $p \in \Pi_r(\mathbb{R}^2)$, since the uniqueness of polynomial $p_\tau(\boldsymbol{x})$, $\tau = 1,\dots,s$.

By appropriately handling (7) we can express the multinode Shepard approximant as follows

$$\mathcal{M}_\nu[f](\boldsymbol{x}) = \sum_{\imath=1}^{n} \mathcal{B}_{\nu,\imath}(\boldsymbol{x})\, f_\imath \tag{8}$$

where, for each $\imath = 1,\dots,n$ we assume

$$\mathcal{B}_{\nu,\imath}(\boldsymbol{x}) = \sum_{\tau\in\mathcal{T}_\imath} K_{\nu,\tau}(\boldsymbol{x})\,\ell_{\tau,\imath}(\boldsymbol{x}). \tag{9}$$

By denoting with $\delta_{\kappa\imath}$ the Kronecker delta function, we observe that

$$\mathcal{B}_{\nu,\imath}(\boldsymbol{\eta}_\kappa) = \delta_{\kappa\imath}, \quad \kappa,\imath = 1,\dots,n, \tag{10}$$

so that the set $\{\mathcal{B}_{\nu,\imath}\}_{\imath=1}^{n}$ is linearly independent on the set $\mathcal{S}$. From now on we refer to $\{\mathcal{B}_{\nu,\imath}\}_{\imath=1}^{n}$ as the multinode cardinal Shepard basis.

In applying the multinode Shepard approximant to numerically solve boundary value problems, it is helpful to rearrange the terms in (8) by splitting them according to the boundary conditions [23]. In the Motz's problem, it is useful a reordering of the nodes in $\mathcal{S}$ as follows

$$\begin{aligned}
&\boldsymbol{\eta}_\kappa \in \Omega, && \kappa = 1,\dots,n_I;\\
&\boldsymbol{\eta}_\kappa \in \Gamma_2\cup\Gamma_4, && \kappa = n_I+1,\dots,n_I+n_{\Gamma_2}+n_{\Gamma_4};\\
&\boldsymbol{\eta}_\kappa \in \Gamma_5, && \kappa = n_I+n_{\Gamma_2}+n_{\Gamma_4}+1,\dots,n_I+n_{\Gamma_2}+n_{\Gamma_4}+n_{\Gamma_5};\\
&\boldsymbol{\eta}_\kappa \in \Gamma_1\cup\Gamma_3, && \kappa = n_I+n_{\Gamma_2}+n_{\Gamma_4}+n_{\Gamma_5}+1,\dots,n,
\end{aligned}$$

where n_I is the number of the interior nodes, n_{Γ_i}, $i = 1,\dots,4$, is the number of nodes on the boundary Γ_i, respectively while n is the total number of nodes.

3. Solution of the Motz's problem through the multinode Shepard method

Let us assume that the approximate solution $\widehat{u}$ of the Motz's problem is expressed as

$$\widehat{u}(\boldsymbol{x}) = \sum_{\imath=1}^{n} \mathcal{B}_{\nu,\imath}(\boldsymbol{x})\,\widehat{u}_\imath, \tag{11}$$

where $\widehat{u}_\imath = \widehat{u}(\boldsymbol{\eta}_\imath)$ are the unknown coefficients and $\boldsymbol{\eta}_\imath$ are the collocation points. By imposing to the approximate solution (11) the interior and the boundary conditions (see equations (1) and (2), respectively), we get a collocation matrix whose entries can be easily computed by taking into account the properties 4-7 satisfied by the functions $K_{\nu,\tau}$ and the Kronecker delta property of the fundamental Lagrange polynomials $\ell_{\tau,\imath}$. More precisely, we obtain

$$\begin{aligned}
A_{\kappa\imath} &= \Delta\mathcal{B}_{\nu,\imath}(\boldsymbol{x})\,|_{\boldsymbol{x}=\boldsymbol{\eta}_\kappa}\\
&= \sum_{\tau\in\mathcal{T}_\imath} \Delta\left(K_{\nu,\tau}(\boldsymbol{x})\,\ell_{\tau,\imath}(\boldsymbol{x})\right)|_{\boldsymbol{x}=\boldsymbol{\eta}_\kappa}\\
&= \sum_{\tau\in\mathcal{T}_\imath} \left(K_{\nu,\tau}(\boldsymbol{\eta}_\kappa)\,\Delta\ell_{\tau,\imath}(\boldsymbol{\eta}_\kappa) + 2\nabla K_{\nu,\tau}(\boldsymbol{\eta}_\kappa)\cdot\nabla\ell_{\tau,\imath}(\boldsymbol{\eta}_\kappa)\right), \qquad \kappa = 1,\dots,n_I,\ \imath = 1,\dots,n,
\end{aligned} \tag{12}$$

$$A_{\kappa\imath} = \frac{\partial\mathcal{B}_{\nu,\imath}}{\partial y}(\boldsymbol{\eta}_\kappa) = \sum_{\tau\in\mathcal{T}_\imath} K_{\nu,\tau}(\boldsymbol{\eta}_\kappa)\,\frac{\partial\ell_{\tau,\imath}}{\partial y}(\boldsymbol{\eta}_\kappa), \qquad \kappa = n_I+1,\dots,n_I+n_{\Gamma_2}+n_{\Gamma_4},\ \imath = 1,\dots,n, \tag{13}$$

$$A_{\kappa\imath} = \frac{\partial\mathcal{B}_{\nu,\imath}}{\partial x}(\boldsymbol{\eta}_\kappa) = \sum_{\tau\in\mathcal{T}_\imath} K_{\nu,\tau}(\boldsymbol{\eta}_\kappa)\,\frac{\partial\ell_{\tau,\imath}}{\partial x}(\boldsymbol{\eta}_\kappa), \qquad \kappa = n_I+n_{\Gamma_2}+n_{\Gamma_4}+1,\dots,n_I+n_{\Gamma_2}+n_{\Gamma_4}+n_{\Gamma_5},\ \imath = 1,\dots,n, \tag{14}$$

$$A_{\kappa\imath} = \mathcal{B}_{\nu,\imath}(\boldsymbol{\eta}_\kappa), \quad \kappa = n_I+n_{\Gamma_2}+n_{\Gamma_4}+n_{\Gamma_5}+1,\dots,n, \quad \imath = 1,\dots,n. \tag{15}$$

By taking into account the Dirichlet boundary conditions (2) on $\Gamma_1\cup\Gamma_3$, we get

$$\widehat{u}_\kappa = u(\boldsymbol{\eta}_\kappa), \quad \kappa = n_I+n_{\Gamma_2}+n_{\Gamma_4}+n_{\Gamma_5}+1,\dots,n.$$

Therefore, the collocation linear system reduces to the order $n_U = n_I+n_{\Gamma_2}+n_{\Gamma_4}+n_{\Gamma_5}$ with

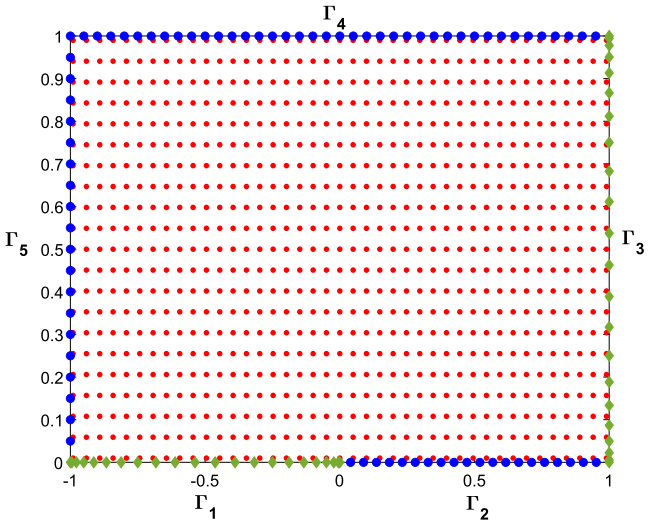

Fig. 2. Set of $n_I = 41 \times 21$ gridded interior points coupled with $n_{\Gamma_1} = n_{\Gamma_3} = 22$ Chebyshev points of the first kind on $[-1, 0]$ and $[0, 1]$ respectively, $n_{\Gamma_2} = n_{\Gamma_5} = 20$ equispaced points on $\left[4 \times 10^{-2}, 1\right)$ and $(0, 1]$ respectively, and $n_{\Gamma_4} = 39$ equispaced points on $(-1, 1)$.

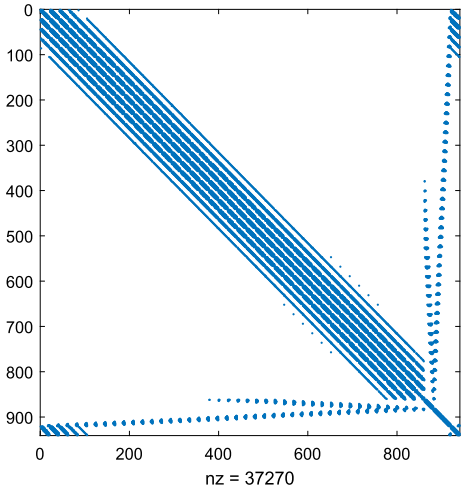

Fig. 3. Sparsity pattern of the collocation matrix related to the points distribution of Fig. 2.

$$
\begin{aligned}
&A_{\kappa\iota} = \Delta \mathcal{B}_{\nu,\iota}(\boldsymbol{x})\,|_{\boldsymbol{x}=\boldsymbol{\eta}_\kappa}, && \kappa = 1, \dots, n_I,\ \iota = 1, \dots, n_U \\
&A_{\kappa\iota} = \frac{\partial \mathcal{B}_{\nu,\iota}}{\partial y}\left(\boldsymbol{\eta}_\kappa\right), && \kappa = n_I + 1, \dots, n_I + n_{\Gamma_2} + n_{\Gamma_4},\ \iota = 1, \dots, n_U \\
&A_{\kappa\iota} = \frac{\partial \mathcal{B}_{\nu,\iota}}{\partial x}\left(\boldsymbol{\eta}_\kappa\right), && \kappa = n_I + n_{\Gamma_2} + n_{\Gamma_4} + 1, \dots, n_U,\ \iota = 1, \dots, n_U,
\end{aligned}
\tag{16}
$$

and known term

$$
\begin{aligned}
&y_\kappa = -\sum_{\iota=n_U+1}^{n} \Delta \mathcal{B}_{\nu,\iota}(\boldsymbol{x})\,|_{\boldsymbol{x}=\boldsymbol{\eta}_\iota} u(\boldsymbol{\eta}_\iota), && \kappa = 1, \dots, n_I, \\
&y_\kappa = -\sum_{\iota=n_U+1}^{n} \frac{\partial \mathcal{B}_{\nu,\iota}}{\partial y}\left(\boldsymbol{\eta}_\iota\right) u(\boldsymbol{\eta}_\iota), && \kappa = n_I + 1, \dots, n_I + n_{\Gamma_2} + n_{\Gamma_4}, \\
&y_\kappa = -\sum_{\iota=n_U+1}^{n} \frac{\partial \mathcal{B}_{\nu,\iota}}{\partial x}\left(\boldsymbol{\eta}_\iota\right) u(\boldsymbol{\eta}_\iota), && \kappa = n_I + n_{\Gamma_2} + n_{\Gamma_4} + 1, \dots, n_U.
\end{aligned}
\tag{17}
$$

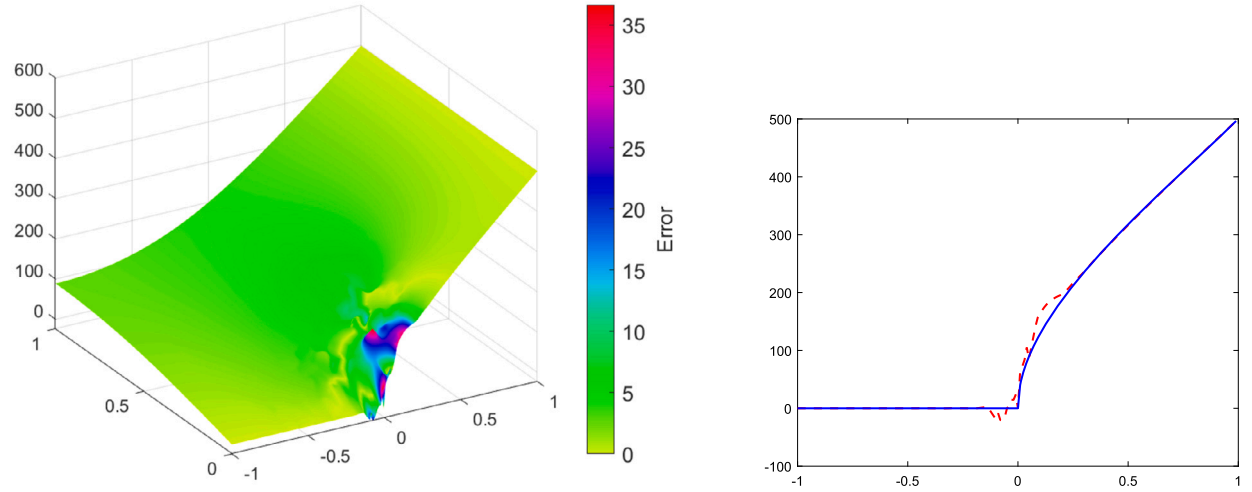

Fig. 4. Error with gridded points and $r = 3$. Left: absolute error on the surface of the approximate solution. Right: approximation behavior along the boundary embedding the singularity. The solid line refers to the 27 terms of the series expansion; the dashed line refers to the multinode Shepard method.

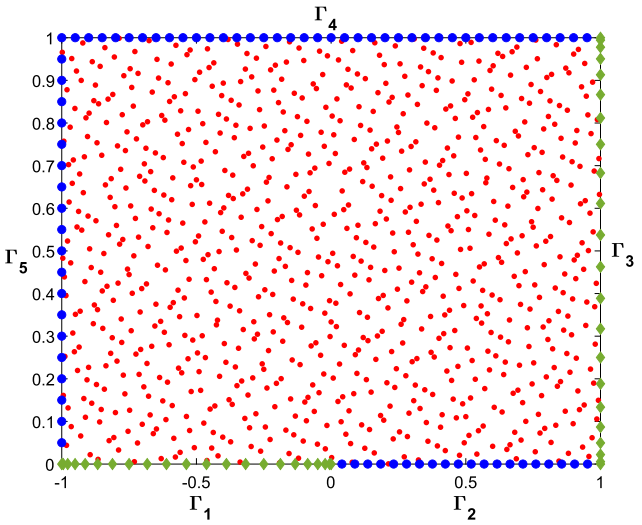

Fig. 5. Set of $n_I = 41 \times 21$ Halton interior points coupled with $n_{\Gamma_1} = n_{\Gamma_3} = 22$ Chebyshev points of the first kind on $[-1, 0]$ and $[0, 1]$ respectively, $n_{\Gamma_2} = n_{\Gamma_5} = 20$ equispaced points on $\left[4 \times 10^{-2}, 1\right)$ and $(0, 1]$ respectively, and $n_{\Gamma_4} = 39$ equispaced points on $(-1, 1)$.

3.1. Numerical experiments

In this section, we perform some numerical experiments to test the approximation accuracy of the proposed method in solving Motz's problem by using different sets of collocation points. We set $\nu = 4$ and, for the computation of the errors, we take as the exact solution the truncation of the series expansion (3) to the first 27 terms.

In the first experiment (see Fig. 2), we consider:

- $n_I = 41 \times 21$ gridded interior points;
- $n_{\Gamma_1} = n_{\Gamma_3} = 22$ Chebyshev points of the first kind on $[-1, 0]$ and $[0, 1]$, respectively;
- $n_{\Gamma_2} = n_{\Gamma_5} = 20$ equispaced points on $[0.04, 0.952]$ and $[0.05, 1]$, respectively;
- $n_{\Gamma_4} = 39$ equispaced points on $[0.95, 0.95]$.

We set $r = 3$ and we generate the covering $\{\gamma_\tau\}_{\tau=1}^{s}$ by considering, for each collocation point $\boldsymbol{\eta}_\iota$, $\iota = 1, \ldots, n$, sets of 17 nearest points ($m = 10$, $q = 7$). The collocation matrix has a sparsity of about 96% and its sparsity pattern is shown in Fig. 3. The absolute error on the surface of the approximate solution is shown in Fig. 4 (left). A maximum absolute error of $3.66e + 1$ and a root mean square error of 3.87 are reached. Moreover, in Fig. 4 (right) we display the behavior of the approximation along the boundary embedding the singularity.

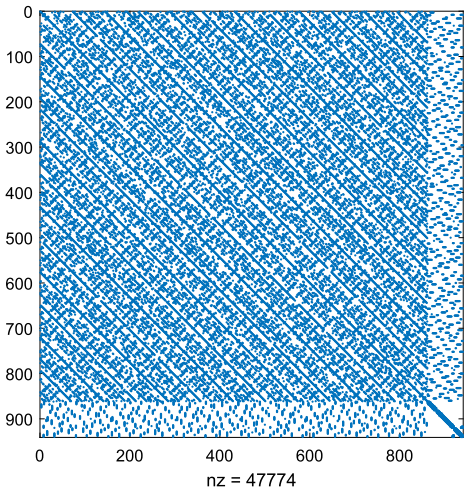

Fig. 6. Sparsity pattern of the collocation matrix for points distribution of Fig. 5.

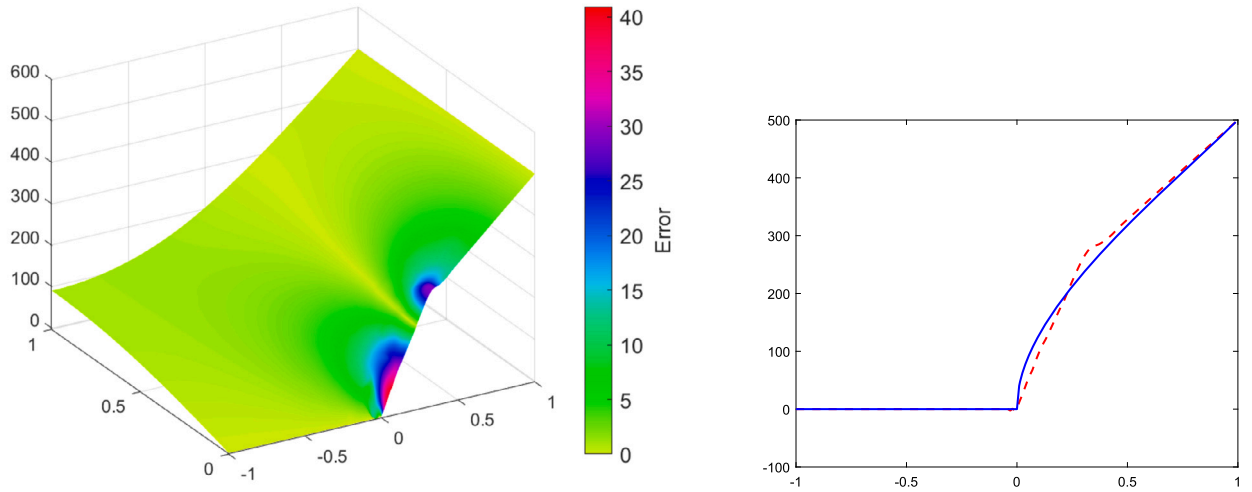

Fig. 7. Error with Halton points and $r = 4$. Left: absolute error on the surface of the approximate solution. Right: approximation behavior along the boundary embedding the singularity. The solid line refers to the 27 terms of the series expansion; the dashed line refers to the multinode Shepard method.

A second experiment has been performed with a set of $n_I = 41 \times 21$ Halton points in $(0,1)^2$ moved into $(-1,1) \times (0,1)$ by means of the affine map

$$(x, y) \mapsto (2x - 1, y), \quad (x, y) \in \mathbb{R}^2 \tag{18}$$

coupled with the boundary points of the first experiment (see Fig. 5). We set $r = 4$ and we generate the covering $\{\gamma_\tau\}_{\tau=1}^{s}$ by considering, for each collocation point $\boldsymbol{\eta}_i$, $i = 1, \ldots, n$, sets of 18 nearest points ($m = 15$, $q = 3$). The collocation matrix has a sparsity of about 95% and its sparsity pattern is shown in Fig. 6. The absolute error on the surface of the approximate solution is displayed in Fig. 7 (left). In particular, we obtain a maximum absolute error of $4.08e + 1$ and a root mean square error of 3.98. Moreover, in Fig. 7 (right) we display the behavior of the approximation along the boundary embedding the singularity.

The presented numerical results show that the multinode Shepard collocation method is not so accurate near the singular point. The loss of accuracy is because the exact solution presents a singularity at the origin which is not captured by the multinode Shepard approximant. In the next Section, we introduce an improvement of the standard methodology to overcome such issue.

4. Solution of the Motz's problem through the enriched Multinode Shepard method

To improve the accuracy of the numerical solution, in line with [32], we need to avoid the oscillations occurring near the singular point. To this aim, it is convenient to enlarge the functional space spanned by the multinode cardinal Shepard basis (9) by including functions that are able to capture the singularity on the boundary. More precisely, we enrich the functional space with the N functions

Table 2
Values of q for the experiment on gridded data varying the number N of the enrichment functions f_ℓ.

N	29×13			41×21			61×31		
	$m=10$	$m=15$	$m=21$	$m=10$	$m=15$	$m=21$	$m=10$	$m=15$	$m=21$
1	8	13	20	7	8	15	9	12	15
2	6	13	20	8	13	15	8	8	15
3	6	13	20	8	13	14	7	8	15
4	7	12	20	7	13	14	8	8	15
5	7	15	19	7	7	15	8	8	15
6	7	15	19	7	7	15	8	8	15
7	13	12	20	8	7	15	13	8	15
8	13	12	18	7	7	15	11	8	15
9	9	19	17	8	7	15	8	8	15
10	9	20	17	11	7	15	9	9	15
11	9	12	17	11	7	14	9	8	15
12	13	12	15	7	7	14	8	8	14
13	9	12	15	11	7	14	9	12	14
14	9	12	14	10	7	14	11	9	15
15	9	12	11	7	7	15	9	8	15
16	13	12	20	7	7	13	9	8	15
17	13	12	19	11	7	15	8	8	14
18	13	19	11	11	7	13	8	8	15
19	13	19	10	11	7	13	11	8	15
20	13	17	13	7	7	3	11	8	14
21	9	20	14	11	7	10	8	8	15
22	9	20	18	11	7	13	13	9	15
23	9	17	11	11	7	13	13	8	15
24	9	17	14	11	7	13	12	8	15
25	8	12	13	11	7	13	11	8	14
26	10	19	16	11	7	13	11	8	9
27	8	11	19	11	10	7	12	8	14
28	17	16	11	15	6	13	11	8	11
29	14	19	12	15	10	3	11	8	2
30	15	20	14	11	10	12	8	9	14

$$f_\ell(\rho,\theta)=\rho^{\frac{2\ell-1}{2}}\cos\left(\frac{2\ell-1}{2}\theta\right),\quad \ell=1,\dots,N, \tag{19}$$

where ρ and θ are the polar coordinates of the point $\boldsymbol{x}=(x,y)$, that is

$$\rho=\sqrt{x^2+y^2}\quad\text{and}\quad\theta=\arccos\left(\frac{x}{\sqrt{x^2+y^2}}\right).$$

More precisely, the approximate solution of the Motz problem is now represented as

$$\widehat{u}(\boldsymbol{x})=\sum_{i=1}^{n}\sum_{\tau\in\mathcal{T}_i}\mathcal{B}_{\nu,\tau}(\boldsymbol{x})\,\alpha_i+\sum_{\ell=1}^{N}\beta_\ell f_\ell(\rho,\theta). \tag{20}$$

Note that the functions f_ℓ in (19) appear in the exact solution (3) and have a singularity of the first order at the origin, therefore are suitable to reproduce the derivative jump. In particular, for each $\ell=1,\dots,N$, we have

$$\frac{\partial f_\ell}{\partial x}=\frac{2\ell-1}{2}\rho^{\frac{2\ell-5}{2}}\left(x\cos\left(\frac{2\ell-1}{2}\theta\right)+y\sin\left(\frac{2\ell-1}{2}\theta\right)\right),$$
$$\frac{\partial f_\ell}{\partial y}=\frac{2\ell-1}{2}\rho^{\frac{2\ell-5}{2}}\left(y\cos\left(\frac{2\ell-1}{2}\theta\right)-x\sin\left(\frac{2\ell-1}{2}\theta\right)\right),$$

and

$$\frac{\partial^2 f_\ell}{\partial x^2}=\frac{(2\ell-1)(2\ell-3)}{4}\rho^{\frac{2\ell-9}{2}}\left((x^2-y^2)\cos\left(\frac{2\ell-1}{2}\theta\right)+2xy\sin\left(\frac{2\ell-1}{2}\theta\right)\right),$$
$$\frac{\partial^2 f_\ell}{\partial y^2}=\frac{(2\ell-1)(2\ell-3)}{4}\rho^{\frac{2\ell-9}{2}}\left((y^2-x^2)\cos\left(\frac{2\ell-1}{2}\theta\right)-2xy\sin\left(\frac{2\ell-1}{2}\theta\right)\right),$$

then,

$$\Delta f_\ell=0.$$

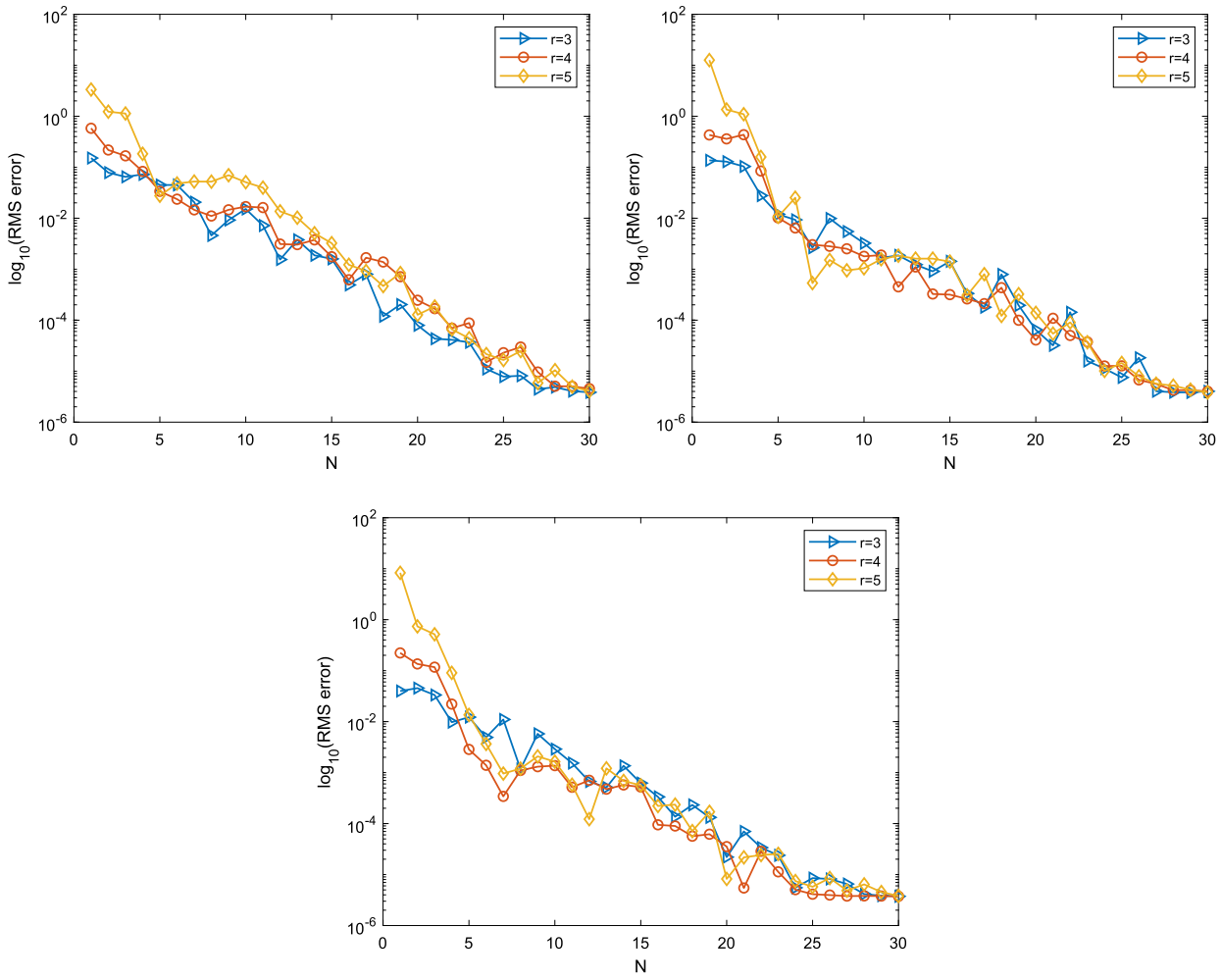

Fig. 8. Root mean square error (in logarithmic scale) on sets of 29×13 interior gridded points (top left), 41×21 interior gridded points (top right), 61×31 interior gridded points (bottom) varying the degree r from 3 to 5.

Consequently, in the collocation process, we have to take into account the conditions related to the enrichment functions f_ℓ which correspond to add N rows and N columns to the collocation matrix. More precisely, the entries of the collocation matrix related to the multinode Shepard operator remain as in (12)-(15) with the addition of the following

$$\begin{aligned} A_{\kappa\iota} &= 0, && \kappa = 1, \dots, n_I, \\ A_{\kappa\iota} &= \frac{\partial f_{\iota-n}}{\partial y}(\boldsymbol{\eta}_\kappa), && \kappa = n_I + 1, \dots, n_I + n_{\Gamma_2} + n_{\Gamma_4}, \\ A_{\kappa\iota} &= \frac{\partial f_{\iota-n}}{\partial x}(\boldsymbol{\eta}_\kappa), && \kappa = n_I + n_{\Gamma_2} + n_{\Gamma_4} + 1, \dots, n_I + n_{\Gamma_2} + n_{\Gamma_4} + n_{\Gamma_5}, \\ A_{k\iota} &= f_{\iota-n}(\boldsymbol{\eta}_\kappa), && \kappa = n_I + n_{\Gamma_2} + n_{\Gamma_4} + n_{\Gamma_5} + 1, \dots, n, \end{aligned} \tag{21}$$

with $\iota = n+1, \dots, n+N$; and finally

$$\begin{aligned} A_{\kappa\iota} &= f_{\iota-n}(\boldsymbol{\eta}_\kappa), && \iota = 1, \dots, n_I, \\ A_{\kappa\iota} &= 0, && \iota = n_I + 1, \dots, n_I + N, \end{aligned} \tag{22}$$

with $\kappa = n+1, \dots, n+N$. The known term is

$$y_\kappa = \begin{cases} 0, & \kappa = 0, \dots, n_I, \\ 0, & \kappa = n_I + 1, \dots, n_I + n_{Neu}, \\ 0, & \kappa = n_I + n_{Neu} + 1, \dots, n_I + n_{Neu} + n_{\Gamma_1} \\ 500, & \kappa = n_I + n_{Neu} + n_{\Gamma_1} + 1, \dots, n_I + n_{Neu} + n_{Dir}, \\ 0, & \kappa = n_I + n_{Neu} + n_{Dir} + 1, \dots, n_I + n_{Neu} + n_{Dir} + N, \end{cases}$$

where $n_{Neu} = n_{\Gamma_2} + n_{\Gamma_4} + n_{\Gamma_5}$ and $n_{Dir} = n_{\Gamma_1} + n_{\Gamma_3}$.

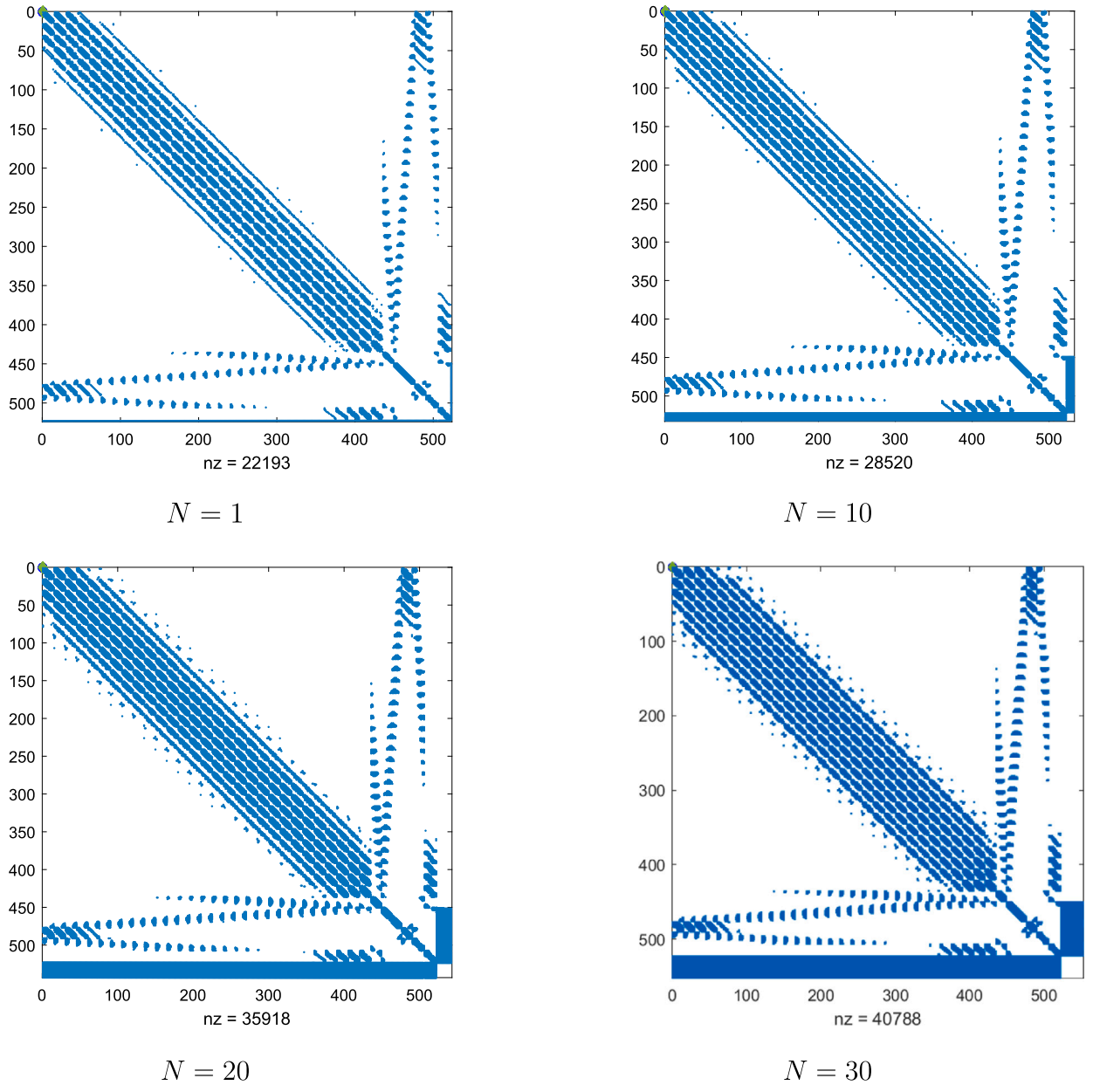

Fig. 9. Sparsity pattern of the collocation matrix for the case $n_I = 29 \times 15$ interior gridded points with $r = 3$ and $N = 1$ enrichment function (top left), $N = 10$ enrichment functions (top right), $N = 20$ enrichment functions (bottom left) and $N = 30$ enrichment functions (bottom right).

4.1. Numerical experiments

In this section, we assess the effectiveness of the enriched multinode Shepard collocation method. Various experiments are conducted on different data sets by varying the number of enrichment functions f_ℓ. The series expansion (3) with the first 27 terms is considered as the exact solution. All the experiments are performed by considering the following sets of points

- $n_I = 29 \times 15$ gridded or Halton points, $n_{\Gamma_1} = n_{\Gamma_3} = 16$ Chebyshev points of the first kind on $[-1, 0]$ and $[0, 1]$, $n_{\Gamma_4} = 27$ equispaced points on $[-0.928, 0.928]$, $n_{\Gamma_2} = n_{\Gamma_5} = 14$ equispaced points on $[0.04, 0.931]$ and $[0.071, 1]$, respectively;
- $n_I = 41 \times 21$ gridded or Halton points, $n_{\Gamma_1} = n_{\Gamma_3} = 22$ Chebyshev points of the first kind on $[-1, 0]$ and $[0, 1]$, $n_{\Gamma_4} = 39$ equispaced points on $[-0.95, 0.95]$, $n_{\Gamma_2} = n_{\Gamma_5} = 20$ equispaced points on $[0.04, 0.952]$ and $[0.05, 1]$, respectively;
- $n_I = 61 \times 31$ gridded or Halton points, $n_{\Gamma_1} = n_{\Gamma_3} = 32$ Chebyshev points of the first kind on $[-1, 0]$ and $[0, 1]$, $n_{\Gamma_4} = 59$ equispaced points on $[-0.966, 0.966]$, $n_{\Gamma_2} = n_{\Gamma_5} = 30$ equispaced points on $[0.04, 0.968]$ and $[0.033, 1]$, respectively.

Table 3
Values of q for the experiment on Halton points varying the number N of the enrichment functions f_ℓ.

N	29×13				41×21				61×31			
	$m=10$	$m=15$	$m=21$	$m=28$	$m=10$	$m=15$	$m=21$	$m=28$	$m=10$	$m=15$	$m=21$	$m=28$
1	3	5	8	11	9	3	12	4	9	13	6	4
2	3	19	8	15	9	20	5	3	9	14	11	4
3	3	19	8	15	9	10	5	3	9	14	11	4
4	3	6	8	10	5	3	5	3	7	14	11	4
5	6	6	3	15	5	6	10	4	7	6	11	4
6	6	6	3	4	5	6	10	3	7	6	11	4
7	6	6	2	11	9	6	3	3	13	7	11	4
8	6	6	2	11	5	6	3	3	6	8	11	4
9	2	6	3	11	9	6	9	3	4	8	4	4
10	5	1	3	11	4	4	15	7	8	8	12	14
11	3	6	3	4	9	6	4	2	8	8	5	6
12	3	6	3	11	5	4	3	20	6	5	4	4
13	17	3	3	11	6	6	6	2	9	6	5	4
14	6	1	3	11	5	6	7	2	9	5	6	4
15	3	3	3	4	6	6	14	12	7	6	3	4
16	3	3	3	11	6	4	4	2	6	6	5	14
17	3	8	3	3	5	6	7	5	9	6	5	6
18	3	2	3	3	4	6	7	4	15	4	5	17
19	3	1	3	5	5	12	3	5	12	6	4	4
20	3	1	3	1	5	4	4	16	6	8	7	4
21	6	3	3	6	7	12	3	4	4	7	5	8
22	3	5	6	3	13	8	3	8	4	6	7	8
23	6	3	3	12	13	19	3	8	4	6	3	8
24	3	3	3	13	13	3	3	7	6	8	5	8
25	6	1	3	6	4	6	2	15	18	8	5	6
26	3	5	8	6	17	6	12	3	16	17	3	10
27	3	1	3	6	8	6	2	15	18	8	3	6
28	3	5	3	6	8	19	2	15	4	5	3	18
29	3	3	2	16	4	6	7	3	9	10	7	4
30	9	3	4	16	4	6	7	3	9	10	7	4

First simulations are performed with the degree r of the local polynomial approximant varying from 3 to 5 and with the values of q as reported in Table 2. In Fig. 8 we display the semilog plot of the root mean square error by varying the number of enrichment functions N from 1 to 30. We observe that the enriched method overcomes the standard one getting better as r and N increase. In Fig. 9 we report the sparsity pattern of the collocation matrix for the case $n_I = 29\times15$ with $N = 1, 10, 20, 30$. According to the equations (21)-(22), we observe that, by increasing the number N of functions f_ℓ, the sparsity pattern of the collocation matrix is about the same.

By varying the point distributions in the problem domain the good behavior of the enriched solution is confirmed. We consider sets of n_I interior Halton points in $(0,1)^2$ moved into $(-1,1)\times(0,1)$ by means of the affine map (18). We set $r = 3,4,5,6$ and we realize the covering $\{\gamma_\tau\}_{\tau=1}^{s}$ by taking into account the values of q as in Table 3. In Fig. 10 we display the semilog plot of the root mean square error varying N and in Fig. 11 we report the sparsity pattern of the collocation matrix for the case $n_I = 29\times15$ with $N = 1, 10, 20, 30$.

5. Conclusion

In this paper the multinode Shepard method has been adopted to solve the Motz problem. This benchmark gives evidence that the standard method is not sufficiently accurate in solving problems with singularity on the boundary. In order to improve the approximation accuracy, the functional space spanned by the multinode cardinal Shepard basis has been enriched by including functions able to capture the discontinuity in the boundary conditions. The performance of the proposed approach improves by increasing both the number of enriched functions and the degree of the local polynomial approximant. Studies with gridded and scattered point distributions are conducted highlighting the numerical behavior of the standard and the enriched multinode Shepard method. Future works are oriented to apply the enriched multinode Shepard method to solve real problems with singularities in the boundary.

CRediT authorship contribution statement

Francesco Dell'Accio: Writing – original draft, Validation, Software, Methodology, Investigation, Formal analysis, Conceptualization. **Filomena Di Tommaso:** Writing – original draft, Validation, Software, Methodology, Investigation, Formal analysis, Conceptualization. **Elisa Francomano:** Writing – original draft, Validation, Software, Methodology, Investigation, Formal analysis, Conceptualization.

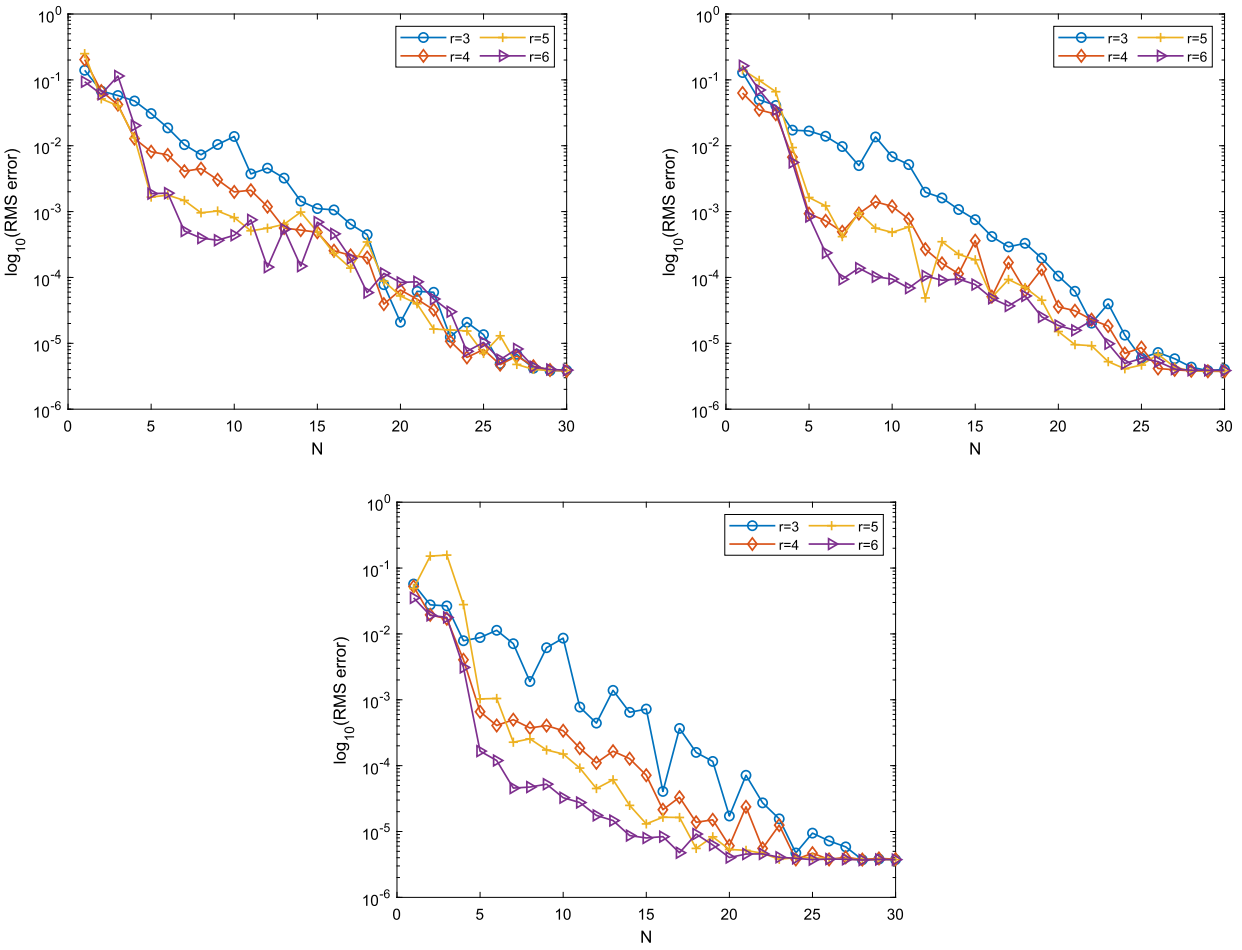

Fig. 10. Root mean square error (in logarithmic scale) on sets of 29×13 interior Halton points (top left), 41×21 interior Halton points (top right), 61×31 interior Halton points (bottom) varying the degree r from 3 to 6.

Acknowledgements

This research has been achieved as part of RITA "Research ITalian network on Approximation", as part of the UMI group "Teoria dell'Approssimazione e Applicazioni" and was supported by INDAM-GNCS projects 2024 and by the FFR 2024 UNIPA. The authors are members of the INdAM Research group GNCS.

References

[1] H. Motz, The treatment of singularities of partial differential equations by relaxation methods, Q. Appl. Math. 4 (4) (1947) 371–377.
[2] Z.-C. Li, R. Mathon, P. Sermer, Boundary methods for solving elliptic problems with singularities and interfaces, SIAM J. Numer. Anal. 24 (3) (1987) 487–498.
[3] R. Wait, A. Mitchell, Corner singularities in elliptic problems by finite element methods, J. Comput. Phys. 8 (1) (1971) 45–52.
[4] F. Bernal, M. Kindelan, Radial basis function solution of the Motz problem, Eng. Comput. 27 (5) (2010) 606–620.
[5] J.B. Rosser, N. Papamichael, A power series solution of a harmonic mixed boundary value problem, Technical Summary Report No. 1405, Mathematics Research Center, University of Wisconsin-Madison, 1975.
[6] G.C. Georgiou, L. Olson, Y.S. Smyrlis, A singular function boundary integral method for the Laplace equation, Commun. Numer. Methods Eng. 12 (2) (1996) 127–134.
[7] C. Xenophontos, M. Elliotis, G. Georgiou, A singular function boundary integral method for Laplacian problems with boundary singularities, SIAM J. Sci. Comput. 28 (2) (2006) 517–532.
[8] T. Lu, H. Hu, Z. Li, Highly accurate solutions of Motz's and the cracked beam problems, Eng. Anal. Bound. Elem. 28 (11) (2004) 1387–1403.
[9] Z. Li, Y. Chan, G. Georgiou, C. Xenophontos, Special boundary approximation methods for Laplace equation problems with boundary singularities— applications to the Motz problem, Comput. Math. Appl. 51 (1) (2006) 115–142.
[10] L. Woods, The relaxation treatment of singular points in Poisson's equation, Q. J. Mech. Appl. Math. 6 (2) (1953) 163–185.
[11] Z. Yosibash, M. Arad, A. Yakhot, G. Ben-Dor, An accurate semi-analytic finite difference scheme for two-dimensional elliptic problems with singularities, Numer. Methods Partial Differ. Equ. 14 (3) (1998) 281–296.
[12] G. Fix, Higher-order Rayleigh-Ritz approximations, J. Math. Mech. 18 (7) (1969) 645–657.
[13] L.G. Olson, G.C. Georgiou, W.W. Schultz, An efficient finite element method for treating singularities in Laplace's equation, J. Comput. Phys. 96 (2) (1991) 391–410.

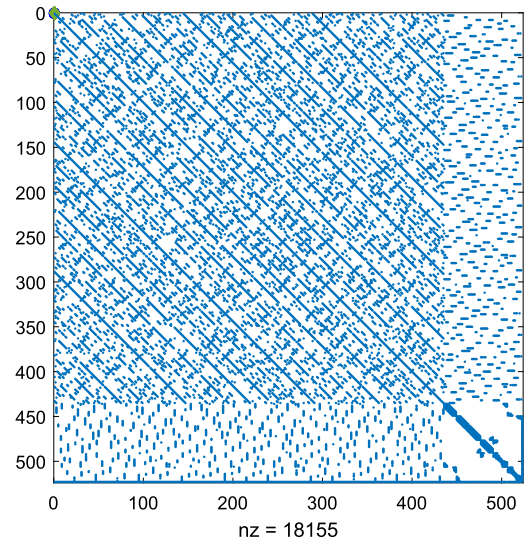

$N = 1$

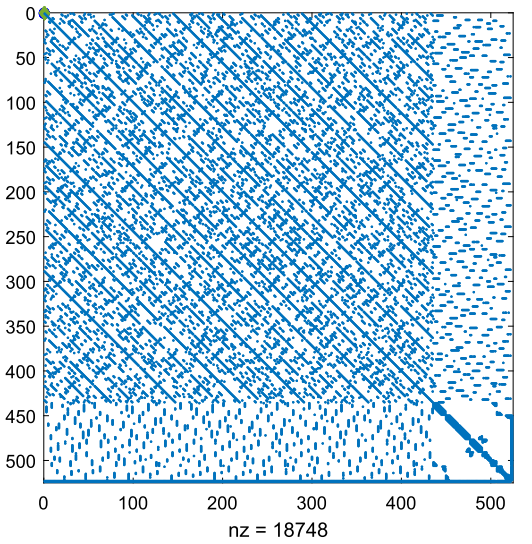

$N = 10$

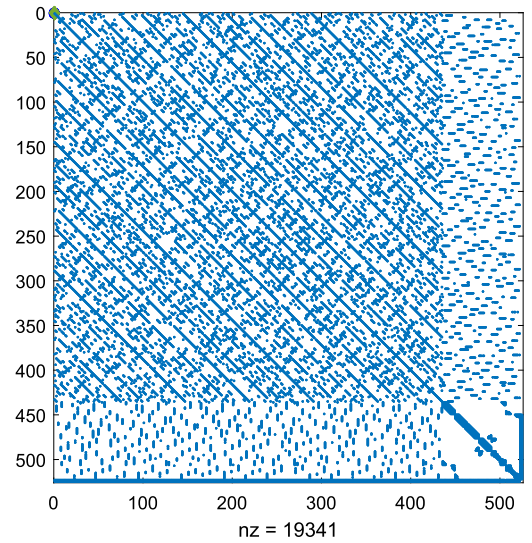

$N = 20$

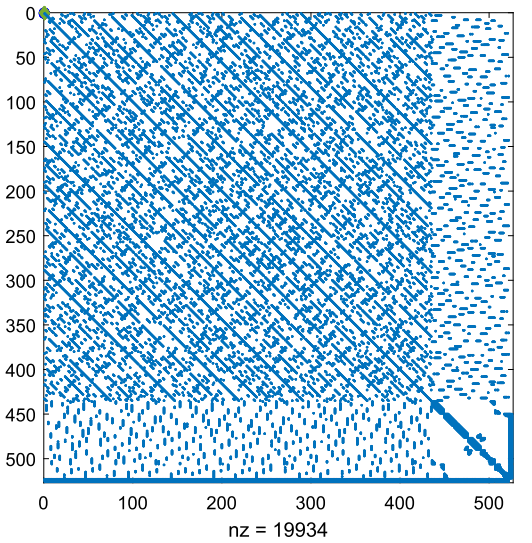

$N = 30$

Fig. 11. Sparsity pattern of the collocation matrix for the case $n_I = 29 \times 15$ interior Halton points with $r = 3$ and $N = 1$ enrichment function (top left), $N = 10$ enrichment functions (top right), $N = 20$ enrichment functions (bottom left) and $N = 30$ enrichment functions (bottom right).

[14] X. Wu, H. Han, A finite-element method for Laplace- and Helmholtz-type boundary value problems with singularities, SIAM J. Numer. Anal. 34 (3) (1997) 1037–1050.
[15] M. Arad, Z. Yosibash, G. Ben-Dor, A. Yakhot, Computing flux intensity factors by a boundary method for elliptic equations with singularities, Commun. Numer. Methods Eng. 14 (7) (1998) 657–670.
[16] M. Elliotis, G. Georgiou, C. Xenophontos, The solution of Laplacian problems over L-shaped domains with a singular function boundary integral method, Commun. Numer. Methods Eng. 18 (3) (2002) 213–222.
[17] D. Ingham, P. Heggs, M. Manzoor, The numerical solution of plane potential problems by improved boundary integral equation methods, J. Comput. Phys. 42 (1) (1981) 77–98.
[18] M. Buhmann, J. Jäger, Quasi-Interpolation, Cambridge Monographs on Applied and Computational Mathematics, Cambridge University Press, 2022.
[19] H. Wendland, Scattered Data Approximation, Cambridge University Press, 2010.
[20] G. Fasshauer, M. McCourt, Kernel-Based Approximation Methods Using Matlab, World Scientific, 2015.
[21] E. Francomano, M. Paliaga, Highlighting numerical insights of an efficient SPH method, Appl. Math. Comput. 339 (2018) 899–915.
[22] F. Dell'Accio, F. Di Tommaso, Rate of convergence of multinode Shepard operators, Dolomites Res. Notes Approx. 12 (1) (2019) 1–6.
[23] F. Dell'Accio, F. Di Tommaso, E. Francomano, Multinode Shepard method for two-dimensional elliptic boundary problems on different shaped domains, J. Comput. Appl. Math. 448 (2024) 115896.

[24] F. Dell'Accio, F. Di Tommaso, O. Nouisser, N. Siar, Solving Poisson equation with Dirichlet conditions through multinode Shepard operators, Comput. Math. Appl. 98 (2021) 254–260.
[25] O. Zienkiewicz, R.L. Taylor, The Finite Element Method, 2, McGraw-Hill, New York, 1991.
[26] J.W.Z. Chen, Y. Xu, Higher-order finite volume methods for elliptic boundary value problems, Adv. Comput. Math. 37 (2012) 191–253.
[27] Z.L.H. Hu, A.H. Cheng, Radial basis collocation methods for elliptic boundary value problems, Comput. Math. Appl. 50 (2005) 289–320.
[28] F. Dell'Accio, F. Di Tommaso, Scattered data interpolation by Shepard's like methods: classical results and recent advances, Dolomites Res. Notes Approx. 9 (2018) 32–44.
[29] L. Bos, S. De Marchi, A. Sommariva, M. Vianello, Computing multivariate Fekete and Leja points by numerical linear algebra, SIAM J. Numer. Anal. 48 (5) (2010) 1984–1999.
[30] F. Dell'Accio, A. Sommariva, M. Vianello, Random sampling and unisolvent interpolation by almost everywhere analytic functions, Appl. Math. Lett. (2023) 108734.
[31] F. Dell'Accio, F. Di Tommaso, N. Siar, On the numerical computation of bivariate Lagrange polynomials, Appl. Math. Lett. 112 (2021) 106845.
[32] F. Bernal, G. Gutierrez, M. Kindelan, Use of singularity capturing functions in the solution of problems with discontinuous boundary conditions, Eng. Anal. Bound. Elem. 33 (2) (2009) 200–208.